Title: Open-top light-sheet microscopy for slide-free nondestructive pathology of human specimens

Authors: Adam K. Glaser[1†], Nicholas P. Reder[2†], Ye Chen[1], Erin F. McCarty[2], Chengbo Yin[1], Linpeng Wei[1], Yu Wang[1], Lawrence D. True[2], and Jonathan T.C. Liu[1*]

[1]Department of Mechanical Engineering, University of Washington, Seattle, WA USA.

[2]Department of Pathology, University of Washington, Seattle, WA USA.

*To whom correspondence should be addressed: jonliu@uw.edu.
†These authors contributed equally to this work

One Sentence Summary: Glaser and Reder *et al.* describe an open-top light-sheet microscope designed to image human surgical and biopsy specimens, enabling slide-free nondestructive 3D pathology with broad implications for individual patient care and precision medicine.

Supplementary Information

Materials and Methods

Figures

Tables

Videos

References

Supplementary Information

Materials and Methods

Collection and processing of fresh mouse tissue

A single mouse (Strain: NCRNU - RF NCRNU-sp/wt, Sex: Male, Age: 8 weeks) was anesthetized with isoflurane and decapitated. Tongue and kidney were harvested from the freshly sacrificed mouse, stained with 1 mM acridine orange for 20 sec, rinsed in phosphate-buffered solution (PBS) for 10 sec, blotted dry, and immediately imaged.

Human prostate core-needle biopsy immunostaining

Prostate core-needle biopsies were incubated in a solution of DAPI with a 1:100 v/v solution of primary antibody. Either rabbit anti-keratin 8 (CK8) (Catalog # AB32579) or mouse anti-keratin 5 (CK5) (Catalog # AB195381) (Abcam, Cambridge, UK), in 1X PBS containing 2% bovine serum albumin and 0.2% Triton X-100 for 24 hrs, followed by an 8 hr rinse in 1X PBS. The sections were then incubated in 1:100 v/v solution of AlexaFluor 660 conjugated either to goat anti-rabbit IgG (Catalog # A21074) or to goat anti-mouse IgG (Catalog # A21054) (Invitrogen, Carlsbad, CA) in a solution of 0.02 % Tween 20 in 1X PBS for 24 hrs at room temperature, with agitation. Biopsies were then rinsed for 6 hrs in 1X PBS, soaked in refractive index-matching solution (~60% TDE at $n = 1.46$) for 30 min, and imaged.

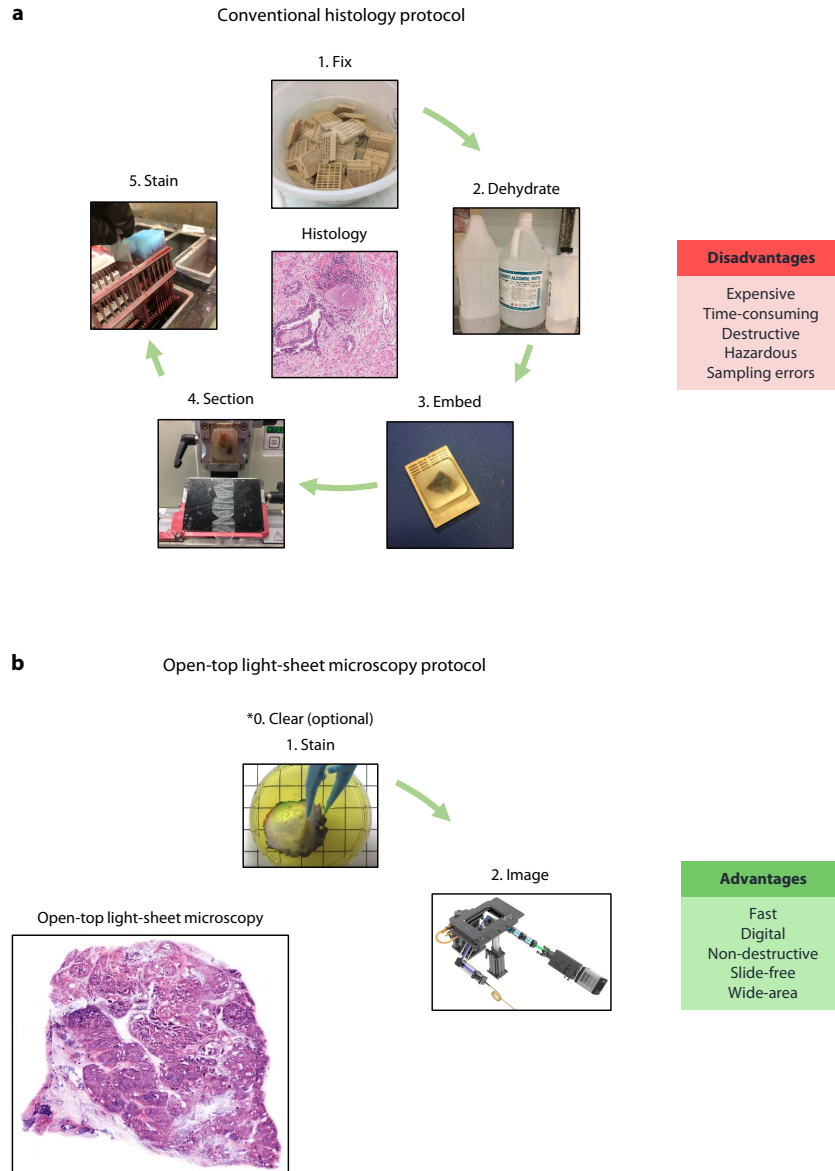*Collection and processing of human kidney tissue*

A 3 x 3 x 0.5 cm piece of de-identified under an IRB-approved protocol, formalin-fixed human kidney tissue was electrophoretically cleared for 48 hrs, at 33 deg C., using a commercially-available tissue clearing system (X-CLARITY, Logos, Annandale, VA). The tissue was then rinsed at room temperature for 8 hrs in 3 changes of 1X PBS with 0.1 % Triton X-100. Refractive index-matching was performed by immersion in TDE (dilute in 1X PBS at $n \sim$ 1.46), for 24 hrs.

Following clearing, the tissue was sequentially immersed in 3% fetal bovine serum in PBST for 24 hrs, rinsed for 48 hrs in 1X PBS with 0.1% Triton X100, and then incubated in the primary antibody solution for 36 hrs, which consisted of an anti-CD31 antibody directly-conjugated to AlexaFluor 700 (Novus Biologicals) (Catalog # FAB3567N), at 1:200 v/v PBS-Tween 20. The tissue was then rinsed for 48 hrs in 3 changes of 1X PBS with 0.1 % Triton X-100.

Collection and processing of human glioma tissue

Human glioma tissues were obtained during neurosurgical resection procedures from consented patients according to an IRB-approved protocol at the Barrow Neurological Institute (St. Joseph's Hospital and Medical Center) in Phoenix, AZ. All patients were orally administered 20 mg/kg body weight 5-ALA (DUSA Pharmaceuticals, Inc.) mixed with 20 mL sterile water 3 hrs prior to surgery. Resected tissues were fixed overnight in 4% paraformaldehyde and stored at 4 deg C in PBS. Prior to open-top light-sheet microscopy imaging of 5-ALA-induced PpIX (a fluorescent porphyrin that preferentially accumulates in glioma cells), the tissues were counterstained with DAPI (1 µg/mL) for 2 min to highlight the cellular nuclei.

Figures

a Conventional histology protocol

1. Fix

5. Stain

Histology

2. Dehydrate

Disadvantages
Expensive
Time-consuming
Destructive
Hazardous
Sampling errors

4. Section

3. Embed

b Open-top light-sheet microscopy protocol

*0. Clear (optional)

1. Stain

2. Image

Advantages
Fast
Digital
Non-destructive
Slide-free
Wide-area

Open-top light-sheet microscopy

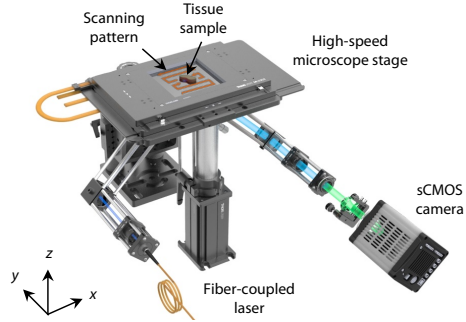**Supplementary Figure 1 |** Conventional histology and open-top light-sheet microscopy protocols

a, The conventional histology protocol requires clinical specimens to be fixed, dehydrated, embedded in paraffin wax, physically sectioned into thin slices, and stained with hematoxylin and eosin (H&E). **b,** With the open-top light-sheet microscope, fresh clinical specimens can be stained and rapidly imaged. In comparison to the conventional histology protocol, the open-top light-sheet microscope is fast, inherently digital, nondestructive, slide-free, and able to provide a wide-area image of the sample, as opposed to a single high-magnification view. Optical clearing is an optional step that may be performed in conjunction with staining to enable deep volumetric microscopy of clinical specimens (e.g. comprehensive volumetric microscopy of entire core-needle biopsies).
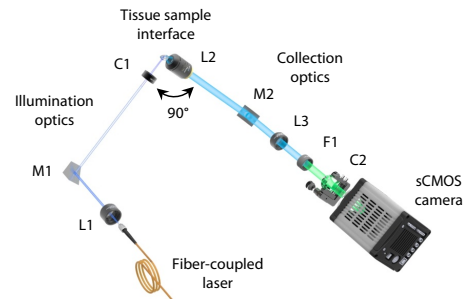
a

Collection axis

Illumination axis

Tissue

Glass

Oil layer

z

x

Solid Immersion lens

b

Collection beam

Illumination beam

z

x

$\theta = 45$ deg.

c

Optically-cleared tissue $\mu_s' = 0.01$ mm^{-1}

Illumination PSF

microns

Collection PSF

Combined PSF

z

x

Fresh tissue $\mu_s' = 1.00$ mm^{-1}

Illumination PSF

microns

Collection PSF

Combined PSF

z

x

x-direction

intensity

$\mu_s' = 0.01$ mm^{-1}
$\mu_s' = 1.00$ mm^{-1}

microns

z-direction

intensity

$\mu_s' = 0.01$ mm^{-1}
$\mu_s' = 1.00$ mm^{-1}

microns

imaging depth

contrast

$\mu_s' = 0.01$ mm^{-1}
$\mu_s' = 1.00$ mm^{-1}

microns

Supplementary Figure 2 | Fractal propagation simulations of the open-top light-sheet microscope

Simulations were performed using a previously published code and methodology [1]. **a,b** Optical schematic of the open-top light-sheet microscope geometry used for simulations. The illumination beam (blue) and collection beam (green) intersect at 90 deg within the sample. **c,** Simulation results are shown for optically cleared tissue, assuming a reduced scattering coefficient of 0.01 mm^{-1}, and for fresh tissue, assuming a reduced scattering coefficient of 1.00 mm^{-1}. The illumination and collection PSFs (beam profiles) are shown, as well as the resulting point spread function (PSF) of the microscope, which is calculated via the adjoint method. Line profiles through the microscope PSF in the x-direction (orange, cleared tissue; red, fresh tissue) and z-direction (cyan, cleared tissue; blue, fresh tissue) are also shown in the bottom row. The predicted contrast as a function of imaging depth in both cleared and fresh tissue is also shown in the bottom right plot.
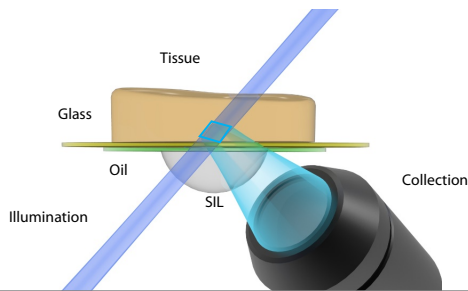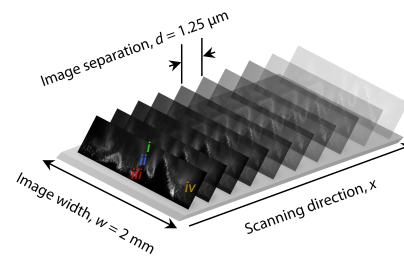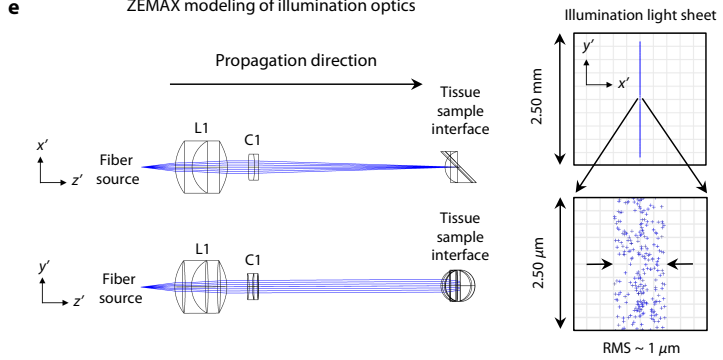
4

a Open-top light-sheet microscope

Scanning pattern
Tissue sample
High-speed microscope stage
sCMOS camera
Fiber-coupled laser
Illumination optics

b Illumination and collection optics

Tissue sample interface
C1
L2
Collection optics
M2
L3
F1
C2
sCMOS camera
Illumination optics
90°
M1
L1
Fiber-coupled laser

c Tissue sample interface

Tissue
Glass
Oil
Illumination
SIL
Collection

d Scanned imaging and field points

Image separation, d = 1.25 μm
Image width, w = 2 mm
Scanning direction, x

e ZEMAX modeling of illumination optics

Propagation direction
L1 C1
Fiber source
Tissue sample interface
L1 C1
Fiber source
Tissue sample interface

Illumination light sheet
2.50 mm
2.50 μm
RMS ~ 1 μm

g Detector spot diagrams of various field points within the light sheet

Circle denotes Airy disk
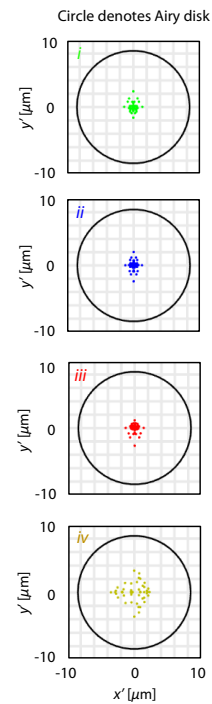
f ZEMAX modeling of collection optics

Propagation direction
C2 L3 L2
Detector
Tissue sample interface
C2 L3 L2
Detector
Tissue sample interface

Field points within the light sheet

5

The design for the open-top light-sheet microscopy system is shown in **a**. The illumination and collection are positioned at 45 deg beneath the sample, which is imaged using a high-speed XY stage and a serpentine scan pattern. The corresponding optics are shown in **b**, where the fiber source, NA = 0.12, is collimated using lens, L1 (f = 25 mm), reflected towards the sample using mirror, M1, and focused to a light sheet using cylindrical lens, C1 (f = 100 mm), resulting in an illumination light sheet with NA ~ 0.03. Fluorescence from the tissue sample is collected using a 4X objective lens, L2 (f = 43.47 mm, NA = 0.28), reflected using mirror, M2, focused through tube lens, L3 (f = 150 mm), and filtered using emission filter, F1. A final low-power cylindrical lens, C2 (f = 2000 mm), is placed before the high-speed sCMOS camera to provide final correction for astigmatism induced as light enters and exits the tissue. The sample interface is shown in **c**, which is comprised of an index-matched solid immersion lens (SIL, n = 1.46), oil, and window interface. A schematic of the acquired images within the sample is shown in **d**. Images are angled at 45 deg, and are captured in succession with an image separation, d, along the scanning direction, x, of the high-speed XY stage. The horizontal size of the image, w, is limited by the field of view of the objective lens, and the vertical size of the image, h, is limited by the depth of focus of the illumination beam. As the illumination light sheet is scanned through the sample, serial fluorescence light sheet images are acquired at a sampling pitch of 1.25 μm. ZEMAX ray-trace modeling of the illumination and collection optics is shown in **e** and **f**, respectively. The illumination optics generate a light sheet that is approximately 2 mm wide and 7 μm thick (diffraction-limited FWHM) at the beam waist. The illumination spot diagram shows minimal blurring of the focal line (~ 1 μm) due to aberrations. Detector spot diagrams are shown in **g**, corresponding to field points originating from various locations within the light sheet, including: ***i***, 250 μm deep into the sample, ***ii***, 125 μm deep into the sample, ***iii*** the surface of the sample, and ***iv***, at the edge of the light sheet, 1 mm from the center and 125 μm deep. The Airy disk represent the size of a diffraction-limited fluorescent point source from the tissue after traveling through the collection arm and being imaged onto the detector (total magnification = 1.46(f_{L3}/f_{L2}) = 5). These spot diagrams show that the imaging of the light sheet (collection path) is essentially diffraction-limited across the entire light sheet.
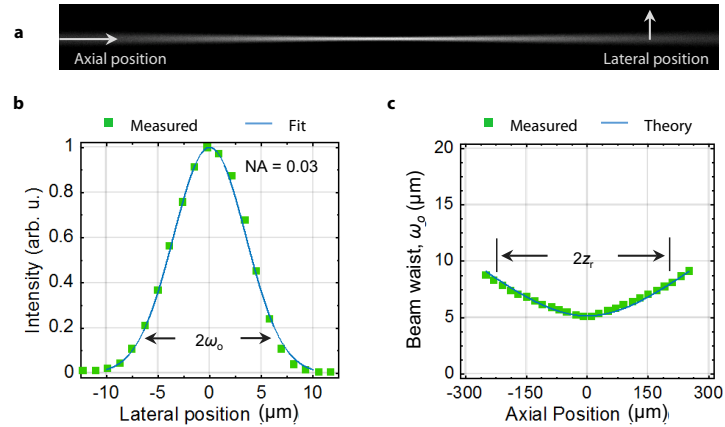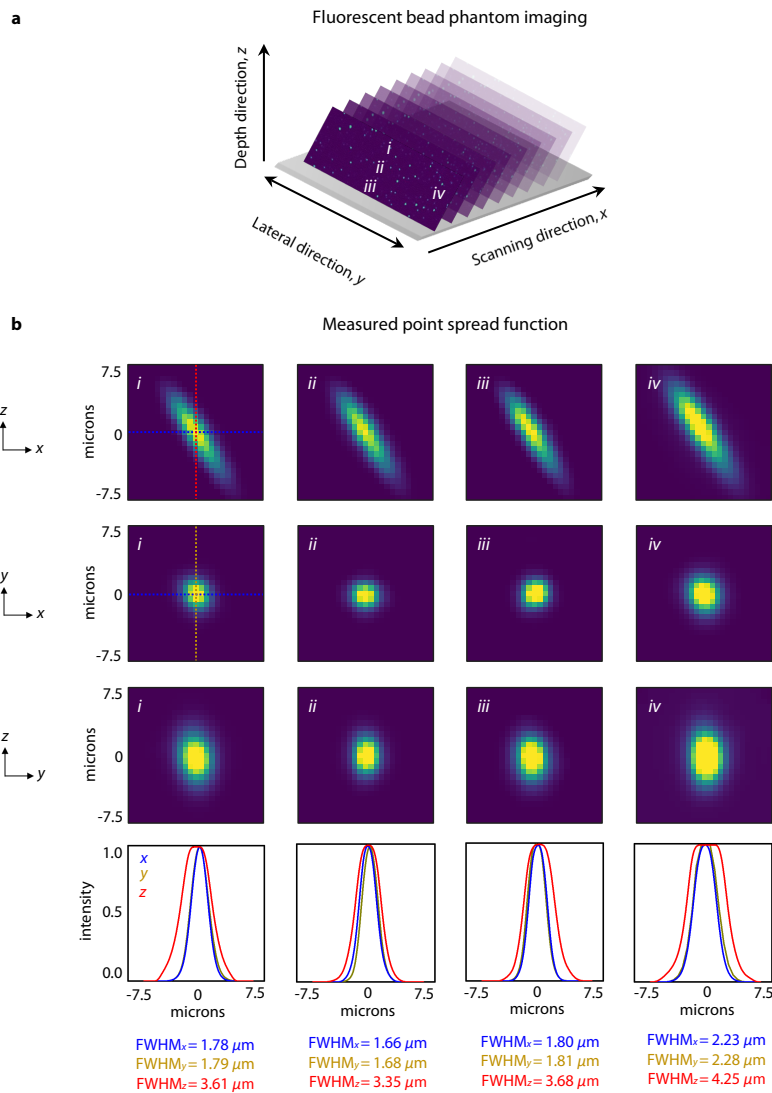
Supplementary Figure 4 | Experimental characterization of the illumination beam

a, Experimental image of the illumination light sheet (λ = 488 nm) with a numerical aperture (NA) of 0.03 in a dilute solution of 1 mM acridine orange. The axial and lateral directions are highlighted. **b,** A lateral intensity profile at the focus of the light sheet. **c,** The radius of the beam waist, ω_o, as a function of axial position. The confocal parameter (twice the Rayleigh range, $2z_R$), is annotated. Both **b** & **c** agree with predictions based on Gaussian-beam theory.
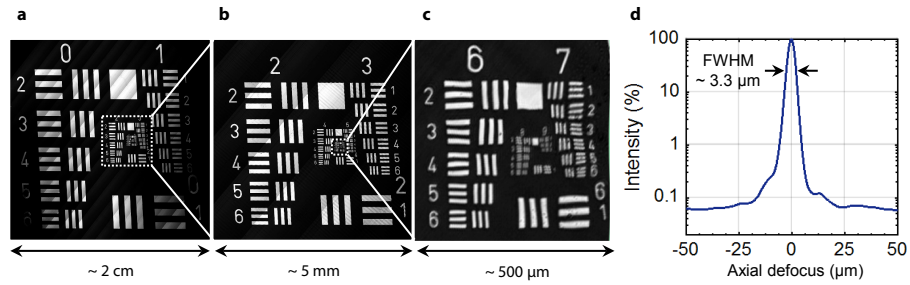
**Supplementary Figure 5 |** Experimental characterization of the open-top light-sheet microscope resolution

a,b,c, Experimental images of a 1951 USAF resolution target at low, medium, and high magnifications. The open-top light-sheet microscope can resolve down to group 8 element 4 corresponding to a resolution of ~1.4 μm. **d,** Axial response of the open-top light-sheet microscope to a flat mirror (log scale).

a Fluorescent bead phantom imaging

b Measured point spread function

FWHM$_x$ = 1.78 μm
FWHM$_y$ = 1.79 μm
FWHM$_z$ = 3.61 μm

FWHM$_x$ = 1.66 μm
FWHM$_y$ = 1.68 μm
FWHM$_z$ = 3.35 μm

FWHM$_x$ = 1.80 μm
FWHM$_y$ = 1.81 μm
FWHM$_z$ = 3.68 μm

FWHM$_x$ = 2.23 μm
FWHM$_y$ = 2.28 μm
FWHM$_z$ = 4.25 μm

**Supplementary Figure 6 |** Experimental characterization of the point spread function

a, A bead phantom was fabricated with 200 nm diameter (sub-resolved) fluorescent beads in a solid agarose phantom and excited at a wavelength of 660 nm. This 3D phantom was imaged using the open-top light-sheet microscope to determine the point spread function of the system. **b,** Beads from four different points (labeled in **a**) within the field of view of the collection objective were analyzed in all three dimensions. Line profiles through these point spread functions are plotted on the bottom row.
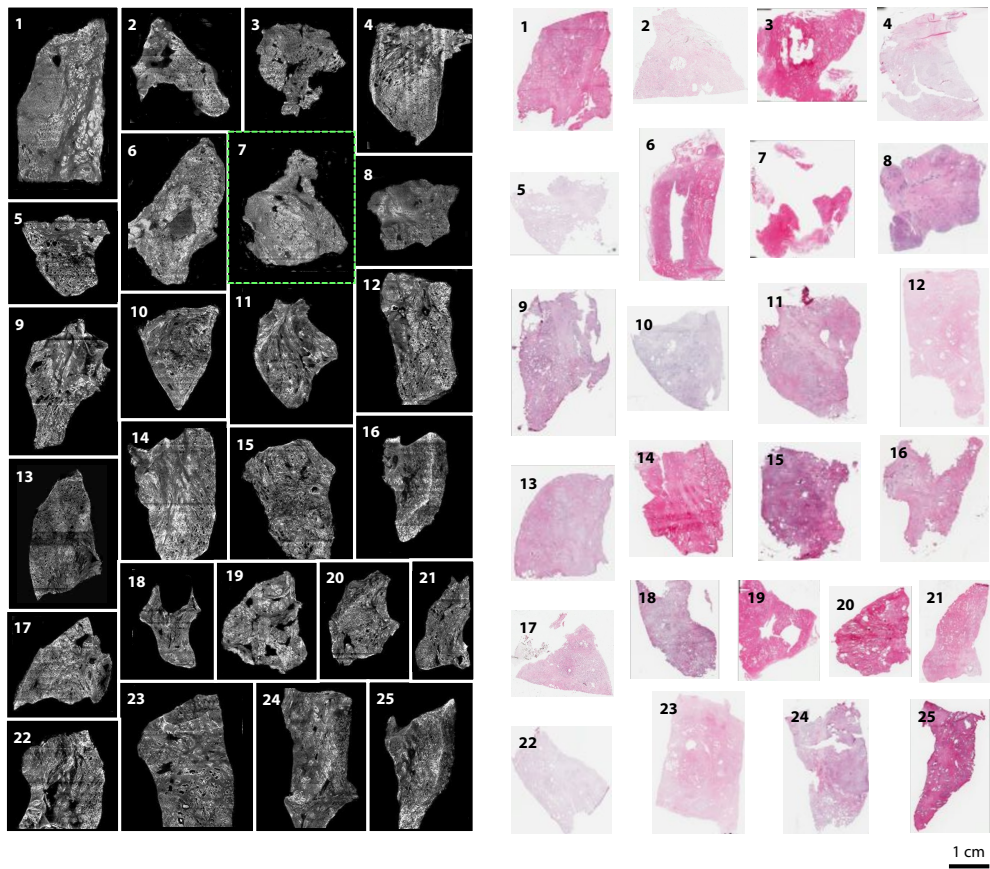
Supplementary Figure 7 | Open-top light-sheet microscopy of N=25 human prostate tissues

Imaging results for all prostate slices imaged for the current study. Surface-extracted open-top light-sheet microscopy images (left) and slide-scanned H&E images of the same tissue surface (right). The highlighted box denotes the prostate slice shown in Fig. 2.

DRAQ5 and eosin dual-channel fluorescent staining and imaging
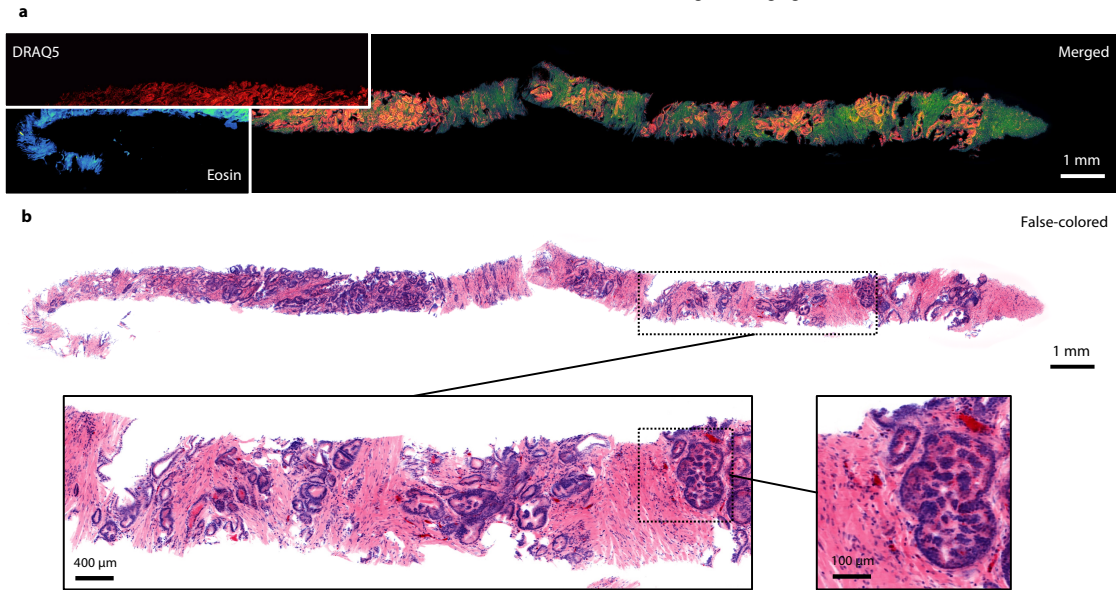
Supplementary Figure 8 | DRAQ5 and eosin dual-channel fluorescence staining and imaging

a, Open-top light-sheet microscopy images of an optically cleared human prostate biopsy, labeled with DRAQ5 (red) and eosin (blue). A composite image of the merged fluorescent channels is shown. In **b,** the fluorescence channels are used as inputs to a nonlinear false-coloring algorithm developed to match the conventional H&E color palette, as also shown in Fig. 4 within the main manuscript.

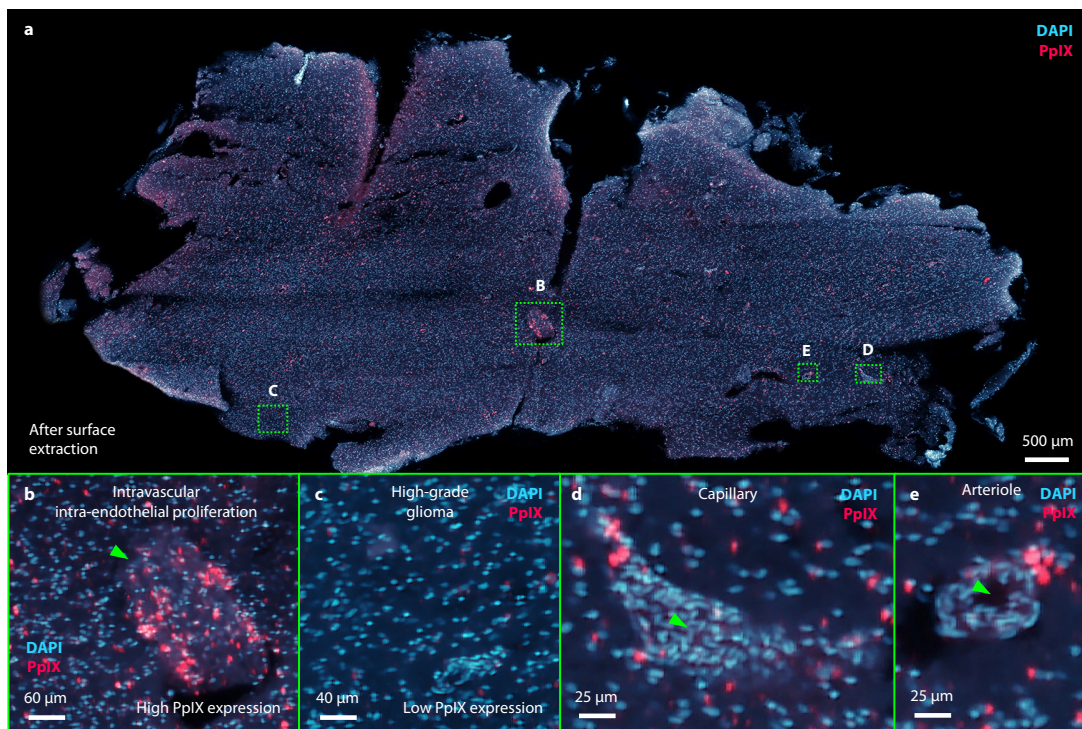Open-top light-sheet microscopy images of mouse kidney
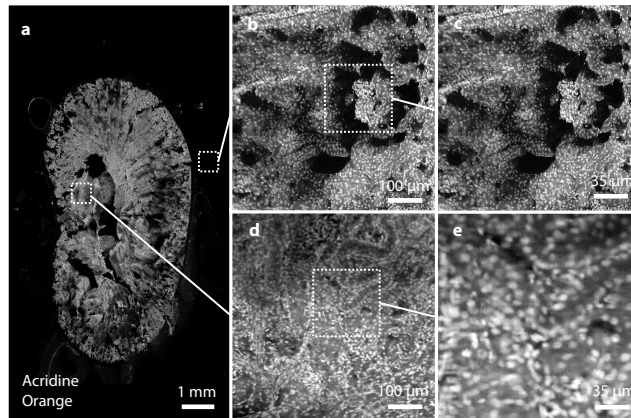
Open-top light-sheet microscopy images of mouse tongue
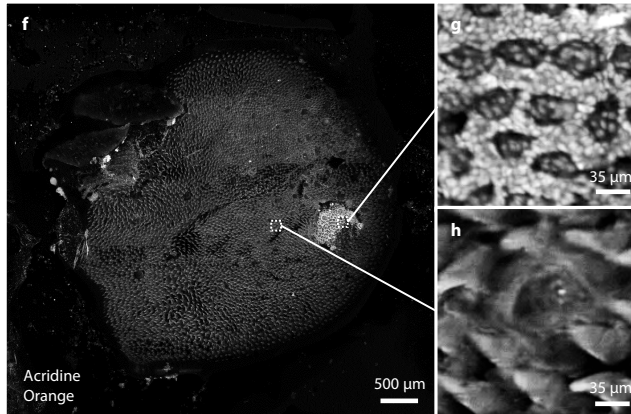
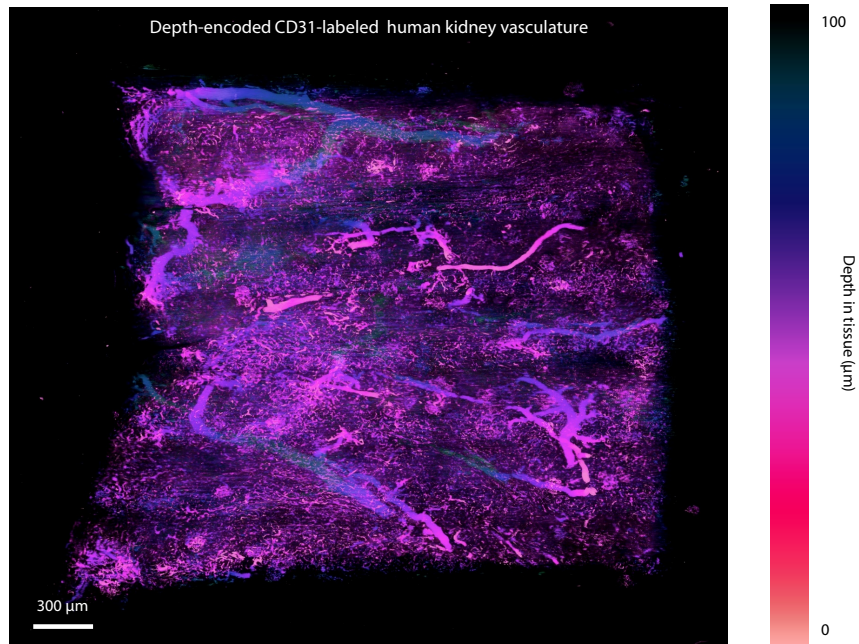**Supplementary Figure 9 |** Open-top light-sheet microscopy images of mouse kidney and tongue

a-e, Images of mouse kidney, and **f-h**, images of mouse tongue, stained with acridine orange at varying levels of magnification. These images demonstrate the utility of the open-top light-sheet microscope for imaging entire mouse organs, and could serve as a vital tool for slide-free, nondestructive pathology in pre-clinical studies.

Open-top light-sheet microscopy of PpIX expression in human brain tumor (high-grade glioma)

Supplementary Figure 10 | Open-top light-sheet microscopy of PpIX expression and DAPI staining in a human brain

a, Dual-channel open-top light-sheet microscopy image of a human brain tumor (glioma). Prior to surgery, the patient was administered 5-ALA, a nonfluorescent pro-drug that is converted into a fluorescent porphyrin (PpIX) that preferentially accumulates in glioma cells. The PpIX fluorescence is shown in red. The nuclei were also counterstained with DAPI (blue) after resection of the tissue (*ex vivo*). Both DAPI and PpIX are excited at 405 nm with the DAPI fluorescence peak at ~460 nm and the PpIX fluorescence peak at ~625 nm. **b,** A higher-magnification view of intravascular intra-endothelial proliferation, with high PpIX expression. **c,** A region of brain tissue with a comparatively low level of PpIX expression. **d-e,** Images of a capillary and arteriole. These images demonstrate the ability of open-top light-sheet microscopy to image a metabolic agent (5-ALA-induced PpIX) that is approved in Europe, and undergoing evaluation by the US FDA, to guide the neurosurgical resection of gliomas. The ability to image these markers in a rapid, slide-free, nondestructive manner could be useful for a variety of fluorescence-guided surgery applications.

Depth-encoded CD31-labeled human kidney vasculature

100

Depth in tissue (μm)

0

300 μm

Supplementary Figure 11 | Open-top light-sheet microscopy of optically cleared CD31-labeled human kidney tissue

Depth-encoded CD31-labeled kidney vasculature channel through a 100-μm thick tissue slice.

Open-top light-sheet immunofluorescence of optically cleared human prostate biopsy
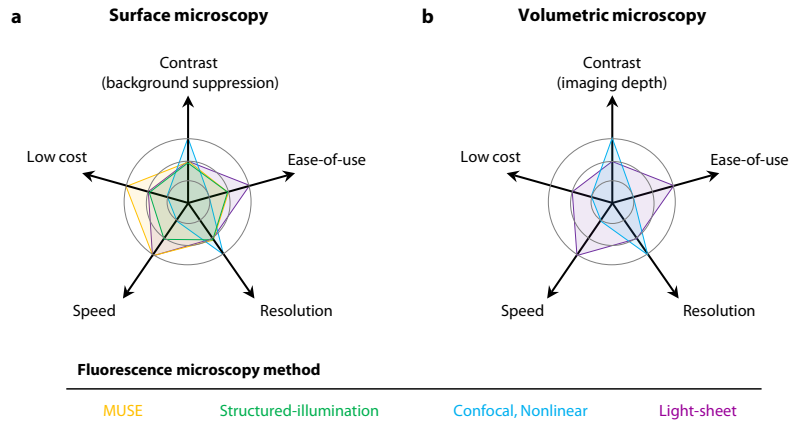
Benign glands   Gleason 4+4 carcinoma

100 µm
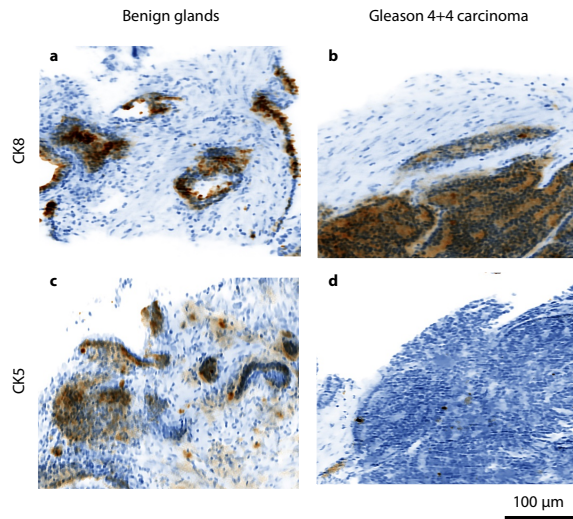
Supplementary Figure 12 | Open-top light-sheet immunofluorescence microscopy of optically cleared human prostate

A core-needle biopsy of a prostate with Gleason 4+4 carcinoma is stained for cytokeratin 8 (CK8) and cytokeratin 5 (CK5) to highlight prostatic epithelial cells and basal cells, respectively. Carcinoma is defined by the absence of a basal cell layer. Both **a**, benign glands and **b**, carcinoma stain for CK8 (epithelial cells lining the lumen). **c**, Benign glands have a CK5-positive basal cell layer beneath the epithelial cells while **d**, carcinoma glands lack a basal cell layer and therefore lack CK5 staining.

Tables

Supplementary Table 1 | Performance tradeoffs for surface and volumetric microscopy of clinical specimens

A summary of some of the key performance features of a selected set of thick-tissue microscopy approaches: MUSE, structured-illumination, confocal, nonlinear, and light-sheet for **a**, surface, and **b**, volumetric microscopy.

Method	Low cost	Ease-of-use	Contrast (2D) / Depth (3D)	Resolution	Speed
MUSE (2D)	*** Requires minimal moving parts or image processing	** Variable focusing required for irregular tissue surfaces	** High contrast only at the surface	*** Limited only by the collection objective	*** Directly acquires 2D surface images. Variable focusing is required for irregular surfaces
Structured-illumination (2D)	** Requires a spatial light modulator, and high-speed camera	** Variable focusing required for irregular tissue surfaces	** Out-of-focus background is digitally removed, limited to surface imaging for most tissues	** Limited by the chosen collection objective and spatial frequency of structured light	** Requires multiple 2D images, which are demodulated. Variable focusing is required for irregular surfaces
Confocal (3D)	* Requires high-speed laser scanning and acquisition	** Moderately complicated to align, optimize, and maintain. Prone to defocusing due to tissue-surface irregularities	*** Pinhole detection results in minimal out-of-focus background	*** Limited only by the collection objective	* Requires pixel-by-pixel laser scanning
Nonlinear (3D)	* Requires high-power pulsed laser source, high-speed laser scanning, and acquisition	* Complicated to align, optimize, and maintain. Prone to defocusing due to tissue surface irregularities	*** Two-photon excitation results in minimal out-of-focus background	*** Limited only by the collection objective	* Requires pixel-by-pixel laser scanning
Light-sheet (3D)	** Requires a sensitive high-speed camera, and high-quality collection objective	*** 3D imaging over a long depth of focus to accommodate irregular tissue surfaces and volumes	** Selective open-top light-sheet illumination, and off-axis collection, results in reduced out-of-focus background	** Limited by the illumination and collection objectives	** (2D) / *** (3D) Directly acquires 2D oblique light sheets for rapid 3D microscopy. No refocusing is required.

Videos

Supplementary Video 1 | Open-top light-sheet microscope demonstration

A video highlighting the ease-of-use and scanning trajectory of the open-top light-sheet microscope. The sample is a fresh prostate tissue slice, stained with 1 mM acridine orange for 20 sec, and rinsed for 10 seconds in 1X PBS.

Supplementary Video 2 | Open-top light-sheet surface microscopy of human prostate tissue

Open-top light-sheet microscopy imaging dataset from a piece of fresh human prostate tissue. High-magnification regions of benign glands and stroma are shown.

Supplementary Video 3 | Open-top light-sheet surface microscopy of fresh human breast tissue

Open-top light-sheet microscopy imaging dataset from a piece of fresh human breast tissue. High-magnification regions of benign lobules and invasive ductal carcinoma are shown.

Supplementary Video 4 | 3D imaging of an optically cleared human prostate core-needle

Volumetric visualization of a human prostate core-needle biopsy with two representative zoomed-in (high-magnification) depth-varying image stacks (sagittal) revealing 3D glandular morphology.

Supplementary Video 5 | 2D e*n-face* z-stack of an optically cleared human prostate core-needle biopsy

Video of a zoomed-in region of a human prostate, in which a stack of depth-varying "sections" is shown (at ~5-µm increments) to mimic a stack of conventional H&E-stained tissue sections of glass slides.

References

1.   Glaser, A.K., Y. Chen, and J.T.C. Liu, *Fractal propagation method enables realistic optical microscopy simulations in biological tissues.* Optica, 2016. **3**(8): p. 861-869.